PROCEEDINGS, Fourtieth Workshop on Geothermal Reservoir Engineering
Stanford University, Stanford, California, February 22-24, 2016
SGP-TR-209

Local Thermal Non-Equilibrium Interfacial Interactions in Heterogeneous Reservoirs - Divergence of Numerical Methods to Simulate the Fluid and Heat Flow

Mario C. Suárez-Arriaga

Mexican Geothermal Association, 58060 Morelia, Mich., México

mcsa50@gmail.com

Keywords: Local thermal non-equilibrium, interfacial interactions, reservoir modeling, finite volume method, averages.

ABSTRACT

This paper focuses on the impact that underground fluid velocity has in numerical algorithms used to model and solve fluid and energy flow problems in heterogeneous geothermal reservoirs. The discussion is based on the energy flow conservation equations for local thermal non-equilibrium conditions. The Integrated Finite Volume method is used here to illustrate this problem. The heat transfer from the solid matrix to the moving fluid at different temperature is modeled for several velocities and global different heat transfers. Especial attention is paid to the dynamic process of cold fluids injected into a reservoir at higher temperature: Water at 50°C is injected into a reservoir at 350°C; if the fluid migrates with constant speed through a permeable corridor from the injection point to a production zone, what is the fluid temperature profile? During the numerical simulation of coupled heat and mass flows in multiple porosity-permeability systems it is necessary to average highly variable physical parameters at the boundaries between different rock domains represented geometrically in a computational mesh. This can be effectively achieved using appropriate average techniques at the contact interfaces of the domains. The averaging process should represent also the correct behavior of the fluid velocity crossing different geologic areas of the reservoir. Therefore, the averages have a decisive influence on the numeric results of the reservoir simulation and in pressure test analysis. Many, if not all, numerical divergence problems arise from the fluid velocity value and the interfacial interactions at the boundaries of different continua. To understand the convergence behavior of the simulated temperature in the injection problem, a new analytical diffusion-convection model was created and its results compared to the finite volume method. A very stable, convergent differencing scheme emerges from this comparison. Two main objectives are achieved herein: the physical reason for the divergence of a numerical model, and the exploration of the range of validity of the local thermal equilibrium hypothesis during the injection of cold water into a hot reservoir.

1. INTRODUCTION

"*The Earth is a heat engine... A highly damped isothermal Earth cannot work. Temperature is the quantity which unlocks the internal energy of the Earth by turning the global system into a highly unstable one. This arises because thermal energy can be transported rapidly by mass transfer and only slowly by thermal diffusion*." John Elder, 1981.

Thermal, mechanical, electrical and transport properties of rocks are determined by their mineralogical composition, chemistry and texture. During the geological development of the reservoir, the primary parameters acquired initial values at different moments of its formation. Later, unpredictable physical processes altered randomly the primary values. In this way porosity, permeability, modules of elasticity, thermal conductivity, heat capacity, density and fluid mobility became heterogeneous. The interrelationships between different petrophysical properties of rocks are extremely complex, and hard to model. Heterogeneities in the fractured matrix allow to consider interaction mechanisms among different media with different porosities and permeabilities. This heterogeneity affects the mass and energy flow and the thermodynamic evolution of the system. The numerical simulation of the coupled heat and mass flow in multiple porosity-permeability systems, needs to average highly variable physical parameters, at the boundaries between different media. The averaging process should represent the fluid crossing different geologic areas of the reservoir, so the averages have a decisive influence on the numeric results of a reservoir simulation in any numerical method. The multiple porosity-permeability concept describes a global interconnected phenomenon that also produces multiple effects on other interdependent phenomena on a larger scale. However, it is not possible to define multiporosity in a unique way. Specific single, double (Cinco Ley & Meng, 1988), triple and multiple porosity-permeability models (Bai *et al*., 1993; Suárez-Arriaga, 2003) have been formulated and used. In this work the attention is focused only on the fluid velocity averaging process when the skeleton and the fluid are at different temperatures. Both phases interact through a volumetric heat transfer mechanism under local thermal non-equilibrium conditions. One key question can be approached with this study: under what conditions the local thermal equilibrium hypothesis is valid? A more general type of interfacial interactions will be considered in the next future.

The main numerical methods traditionally used in numerical reservoir evaluations are Finite Differences (FD), Finite Elements (FEM) and Finite Volumes (FVM). All these numerical schemes need to deal with internal and external boundary conditions. When the physical properties between two boundaries are very different, it is necessary to perform averages of the respective properties existing at each side of the common boundary. Depending on the average formula used, the behavior of mass and energy flows will be different producing frequent numerical divergences. This phenomenon is independent of the numerical method used to simulate the physical processes involved. In this paper, because of the available space, only the FVM is used to illustrate this point. The FVM or Integrated Finite Volumes Method (Patankar, 1980) or Surface Integrated Finite Differences (Narasimhan, 1976) is a kind of generalization of the

finite difference method, which is used in the popular numerical simulator TOUGH2 (Pruess, 1988) and in other computational fluid dynamics software such as ANSYS – CFD / FLUENT/ CFX, PHOENICS, STAR-CD, etc. (Bundschuh & Suárez-Arriaga, 2010). The FVM has the intrinsic ability to represent the main conservation laws of flow in geothermal reservoirs. In this paper it is numerically shown, with a concrete injection example, the convergence behavior of the FVM applied to flow geothermal problems. It is also shown that one of the main divergence problems arises when the flow velocity is higher than a threshold value. The average formula used at the interfaces among neighbors elements will determine the numerical stability and correct convergence of the method to compute accurately and correctly the fluid and heat flow. In this context it is possible to define a Peclet number for porous media relating convection to diffusion. To compute the flow at the boundaries of the reservoir, several averaging formulas are introduced and tested. As a general trend, when the flow velocity increases, the numerical procedure diverges and/or oscillates at high velocities. The final objective is to produce efficient differentiation schemes that are physically realistic, do not produce oscillations and are numerically stable during the simulation of complex flows in geothermal reservoirs.

2. THE CONDUCTION-CONVECTION LOCAL THERMAL NONEQUILIBRIUM MATHEMATICAL MODEL

The general energy flow equation in geothermal reservoirs includes conduction and convection through an advective term related to the transport of heat by the moving fluid phase in the pores and heat conduction in the solid phase, plus an extra term for the energy transfer between the solid and the fluid phases at different temperatures. Under these conditions there is no longer local thermal equilibrium and $T_s \neq T_f$, except at the solid-fluid common boundary $\mathbf{\Gamma}_{sf}$. In local thermal non-equilibrium (LTNE) state, when dispersion, viscous dissipation and radiative effects are negligible, this combined energy transfer process is modeled by the following system of two partial differential equations, one for the solid phase (s) and one for the fluid phase (f), (Nield & Bejan, 2013; Vafai, 2015):

$$\frac{\partial}{\partial t}\Big((1-\varphi) c_s \rho_s T_s \Big) - (1-\varphi)\,\vec{\nabla}\cdot\Big(\mathbf{k}_s \cdot \vec{\nabla} T_s\Big) = (1-\varphi) q_s - (1-\varphi)\, q_{sf}\,(h_V, \Delta T) \qquad \rightarrow \left[\frac{W}{\mathrm{m}^3}\right] \tag{1}$$

$$\frac{\partial}{\partial t}\Big(\varphi c_f \rho_f T_f\Big) \;-\; \varphi\,\vec{\nabla}\cdot\Big(\mathbf{k}_f \cdot \vec{\nabla} T_f\Big) \;+\; \vec{\nabla}\cdot\Big(c_f \rho_f T_f \vec{v}_D\Big) = \varphi\, q_{sf}\,(h_V, \Delta T) \qquad \rightarrow \left[\frac{W}{\mathrm{m}^3}\right] \tag{2}$$

where t, φ, c, ρ, T, $\mathbf{k}$, $\boldsymbol{v}_D$, q_s and q_{sf} are time, porosity, heat capacity, density, temperature, conductivity tensor, Darcy velocity and volumetric heat generation of the solid (s) and fluid (f) phases respectively. The symbol q_{sf} is the amount of volumetric heat transferred from the solid matrix to the fluid and viceversa; $\Delta T = (T_s - T_f)$ is the solid-fluid temperature difference; the volumetric heat q_{sf} depends also on thermal coefficients and geometric variables discussed in the next subsection. The conservation of the fluid mass in the porous rock is:

$$\frac{\partial\big(\varphi \rho_f\big)}{\partial t} + \vec{\nabla}\cdot\Big(\rho_f \vec{v}_D\Big) = 0 \;\rightarrow \left[\frac{\mathrm{kg}}{\mathrm{s}}\frac{1}{\mathrm{m}^3}\right], \;\; \vec{v}_D = \varphi\, \vec{v}_f = -\frac{\mathbf{K}}{\mu_f}\cdot\Big(\vec{\nabla} p - \rho_f\, \vec{\mathrm{g}}\Big) \tag{3}$$

where $\mathbf{K}$, μ_f, p, $\boldsymbol{g}$ are absolute permeability tensor, fluid viscosity, fluid pressure and gravity acceleration, respectively. The microscopic fluid velocity in the pores and fractures $\boldsymbol{v}_f$, is related to the Darcy flux $\boldsymbol{v}_D$ by the Dupuit-Forchheimer relation $v_D = \varphi\, v_f$ (Bear, 1973). Assuming steady state ($\partial/\partial t = 0$), replacing the mass conservation (3) into equation (2), within volumes V_s and V_f of the solid and fluid phases respectively, a steady state LTNE coupled model is obtained:

$$\left(\begin{array}{c} q_{sf} = h_V\,(T_s - T_f)\,, \left[\dfrac{W}{m^3 °C}\right] \\ h_V = \gamma_{sf}\, h_{sf}\,,\; \gamma_{sf} = \dfrac{\Gamma_{sf}}{V_s} \end{array}\right) \rightarrow \left\{\begin{array}{lll} \vec{\nabla}\cdot\left(\dfrac{\mathbf{k}_s}{c_s \rho_s}\cdot\vec{\nabla} T_s\right) = -\dfrac{q_s}{c_s \rho_s} + \dfrac{q_{sf}}{c_s \rho_s} = Q_s & \rightarrow \left[\dfrac{°C}{\mathrm{s}}\right] & (a) \\ \vec{\nabla}\cdot\left(\dfrac{\mathbf{k}_f}{c_f \rho_f}\cdot\vec{\nabla} T_f\right) - \dfrac{\vec{v}_D}{\varphi}\cdot\vec{\nabla} T_f = \dfrac{-q_{sf}}{c_f \rho_f} = -Q_f & \rightarrow \left[\dfrac{°C}{\mathrm{s}}\right] & (b) \end{array}\right\} \tag{4}$$

where h_V (W/m^3/°C) is the volumetric heat transfer coefficient, Q_s and Q_f quantify the global solid-fluid heat transfers, h_{sf} (W/m^2/°C) is the interfacial heat transfer coefficient, coupling the heat equation of the skeleton (1) to the fluid heat equation (2); γ_{sf} is a geometric factor, which is discussed later, and Γ_{sf} (m^2) represents the area of the common solid/fluid boundary (Figure 1).

2.1 The solid-fluid heat transfer coefficient h_{sf}

There are two types of heat transfer coefficients in equation 4, the volumetric coefficient q_V (W/m^3/°C), and the interfacial coefficient h_{sf} (W/m^2 /°C), which is responsible for the energy transfer between the solid matrix and the fluid. This last coefficient can be determined experimentally; for example in a porous bed of spherical particles (Figure 1b), h_{sf} can be estimated with the following formula (Nield & Bejan, 2013; Vafai, 2015):

$$h_{sf} = \frac{6(1-\varphi)}{\big(d_p\big)^2}\left(\frac{1}{Nu\, k_f} + \frac{1}{10\, k_s}\right)^{-1}, \quad Nu = 2.0 + 1.1\Big(Pr^{1/3} Re^{0.6}\Big), \quad Re = \frac{\rho_f\, v_f}{\mu_f} l_0 \leq 100 \;\Rightarrow\; 0.1 \leq Nu \leq 12.4 \tag{5}$$

where d_p is the particle diameter, Nu is the fluid-solid Nusselt number or dimensionless heat flux, (the formula to compute Nu is from Wakao and Kaguei, 1982 *in* Vafai, 2015), Re is the Reynolds number or ratio of inertial to viscous forces, l_0 is a porous rock average characteristic length. The Prandtl number $Pr = c_f \mu_f / k_f$, depends only on fluid properties. The range of validity of Nu in equation (5) is for Re lower than or equal to 100 (Figure 2). Under the same temperature difference, thermal energy flows along paths of high conductivity and least resistance. In geothermal rocks with heat diffusing from below, as in the reinjection case, energy is preferentially transported through zones with increasing fluid velocity. Low conductivity regions act as a retardant to heat flow (Figure 1).

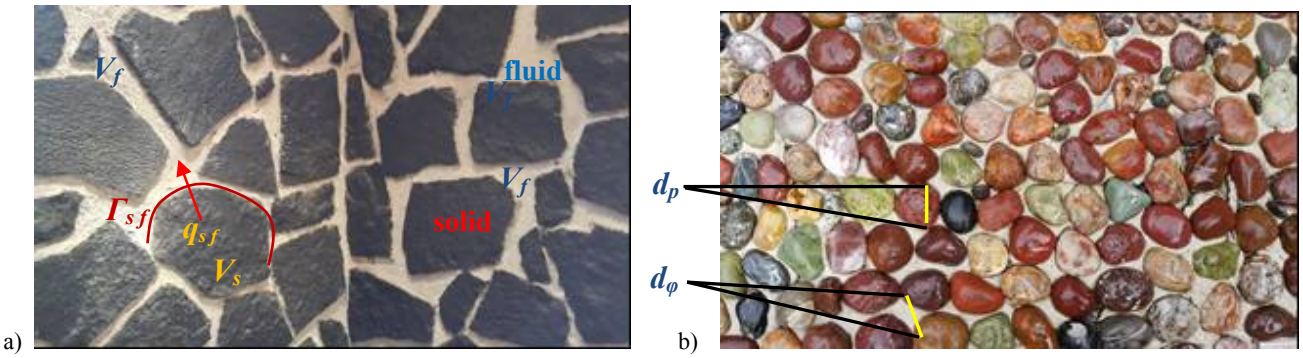

Figure 1: Physical models at different macroscales of porous rocks illustrating the skeleton, the 'fractures', the heat flow q_{sf} and the geometric elements, the fluid-solid contact surface Γ_{sf}, the particle diameter d_p and the pore diameter d_φ. a) wall made with volcanic rocks ($A \sim 1.2$ m^2, $d_p \sim 35$ cm, $d_\varphi \sim 4$ cm); b) floor with rounded stones ($A \sim 0.25$ m^2, $d_p \sim 5$ cm, $d_\varphi \sim 1.5$ cm).

For Darcy velocities in the range [1, 10^4] × 10^{-8} m/s, the flow is laminar and the corresponding Reynolds numbers are always lower then 100; therefore the corresponding Nusselt numbers are in the range [2, 3] (Figure 2), in agreement with the experimental values reported by Nield & Bejan (2013).

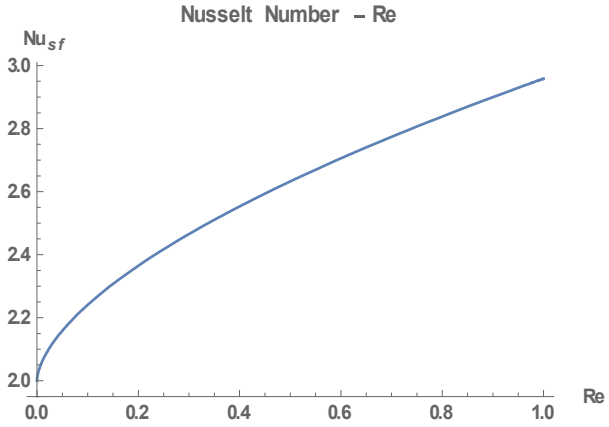

Figure 2: The Nusselt number Nu as a function of the Reynolds number for laminar flow.

Acidic rocks present a volumetric heat generation around 2 × 10^{-6} W/m^3; basic rocks produce heat in the range [10^{-8}, 10^{-7}] W/m^3, (Beardsmore and Cull, 2001). For temperature differences (T_s - T_f) between the rock and the fluid in the range [1, 300] °C, the corresponding heat transfer term $h_V (T_s - T_f)/\rho_f/c_f$ can vary between 10^{-2} and 10^{-7} °C/s, depending on the value of the factor γ_{sf}. The two temperatures can vary within the X-distance; increases in velocity generally result in increases in heat transfer coefficient h_{sf}.

The terms h_V and h_{sf} are included in very simple expressions of equation (4) for the solid-fluid heat transfer, but their physical meaning represent very complex phenomena, which depend on many factors such as fluid and rock properties, distribution and topology of pores, geometry of both, the solid skeleton and the fractures, dimensions and contact area between pores-fractures and matrix (Figure 1). The area Γ_{sf} is very difficult to compute exactly in real reservoirs, because unknown geometrical factors such as γ_{sf}, d_p and d_φ are needed. The unknown geometric factor $\gamma_{sf} = \Gamma_{sf}/V_s$ can be computed exactly only in artificial porous media for very simple contact surfaces. For example in idealized cases, for a perfect spherical particle the ratio $\gamma_{sf} = 6/d_p$; for cylinders $\gamma_{sf} = 4/d_p$, in rectangles $\gamma_{sf} = 1/d_p$, etc. Because of the complicated and almost unknown internal geometry of the pores and fractures themselves, and dimensions of the contact surface Γ_{sf} (Figure 1) and the lack of experimental data, other types of approach need to be used in geothermal porous rocks to estimate correctly the solid-fluid heat transfer in the LTNE model. These approaches could come from numerical deduction in physical-mathematical models.

2.2 A diffusion exact model in 1D

In order to be able to compare the convergence of a numerical solution, an analytical solution is needed for an idealized case. With this purpose, two exact solutions are developed here and in next subsection. Assuming homogeneous properties in the solid matrix, let V_S be the elementary volume representing the skeleton. Thermal energy is diffused by conduction through a two-dimensional domain of rock with negligible or very low porosity as illustrated in figure 3, where the matrix temperature only depends on the vertical coordinate z (m) and the boundary conditions are constant and fixed at the bottom (T_B) and the top (T_A) respectively, with $T_B > T_A$.

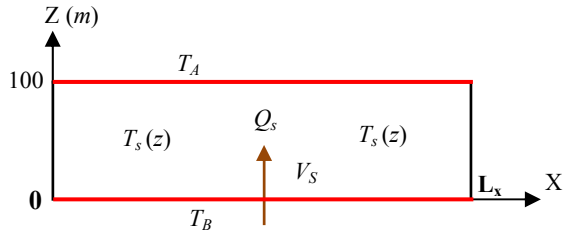

Figure 3: Two-dimensional domain of rock with negligible porosity, L_x represents an arbitrary horizontal length.

In steady-state conditions and homogeneous rock, under appropriate assumptions in 1D, the diffusion model described by equation (4a), with constant boundary conditions in V_S, becomes simply:

$$\frac{d}{dz}\left(\eta_s \frac{dT_s(z)}{dx}\right) = Q_s\,, \quad T_s(z=0)=T_B\,, \quad T_s(z=100)=T_A\,; \quad \eta_s = \frac{k_s}{c_s\,\rho_s} \tag{6}$$

where η_s [m^2/s] is the thermal diffusivity of the solid matrix. Integrating twice equation (6) with its boundary conditions:

$$T_s(z) = T_B + \frac{T_A - T_B}{L} z + \frac{Q_s (z-L)\, z}{2\,\eta_s} \tag{7}$$

Figure 3 shows the vertical distribution of temperature obtained with this pure diffusion model in the range $0 \le Z \le 100$ m, in the interval $350°C \le T \le 370°C$. The continuous line is the exact solution (7), the red points are the approximate solution obtained with the FVM described in section 3. It is evident that the FVM converges to the exact solution even in a coarse mesh of only 10 nodes.

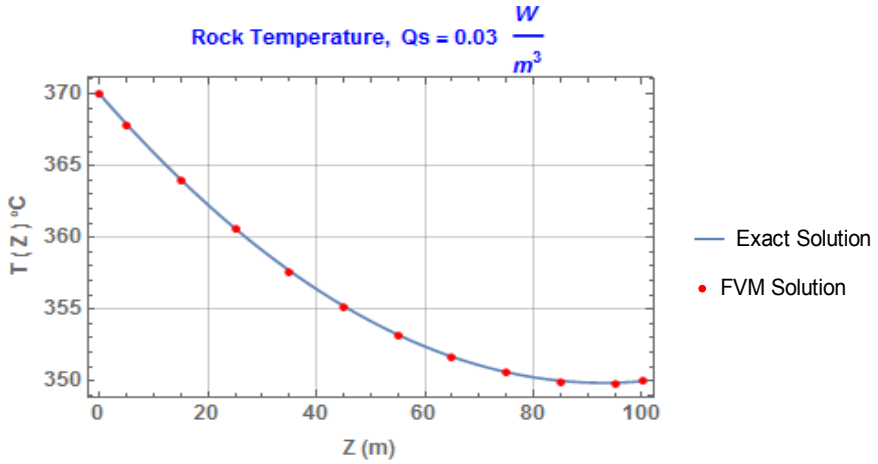

Figure 4: Vertical distribution of temperature obtained from the analytic solution (7) and the FVM solution (12).

It is interesting to notice that a similar temperature distribution can be obtained from the infinite series solution (Figure 5a) of the transient heat flow equation adapted from Carslaw & Jaeger (1959, p. 130), for a time $t_0 = 65$ years $= 2.05124 \times 10^9$ seconds:

$$T_s(z,t_0) = \frac{q_V L^2}{2\,k_A}\left(1 - \frac{z^2}{L^2} - \frac{32}{\pi^3}\sum_{n=0}^{1000}\frac{(-1)^n}{(2n+1)^3}\,\mathrm{Cos}\left[\frac{(2n+1)\,\pi\, z}{2\,L}\right]\mathrm{Exp}\left[-(2n+1)^2\,\pi^2\,\frac{\eta_s}{4\,L^2}\,t_0\right]\right) + 370\ °C \tag{8}$$

where k_A is the effective solid thermal conductivity; in the case of a rock with non-negligible porosity $k_A = (1 - \varphi)\, k_s + \varphi\, k_f$, equation (8) is still valid. This solution corresponds to heat flow in a 1D domain with initial condition $T_s(z\,, 0) = 370$ °C, and symmetrical boundary conditions $T_s(-100, 0) = T_s(100, 0) = 370$ °C. $q_V < 0$ because the rock is cooling in the interval $-100 \le Z \le 0$, for this model. Solution (8) is not valid for early times; for example at $t = 11{,}000$ s it produces oscillations at the domain around the initial condition (Figure 5b).

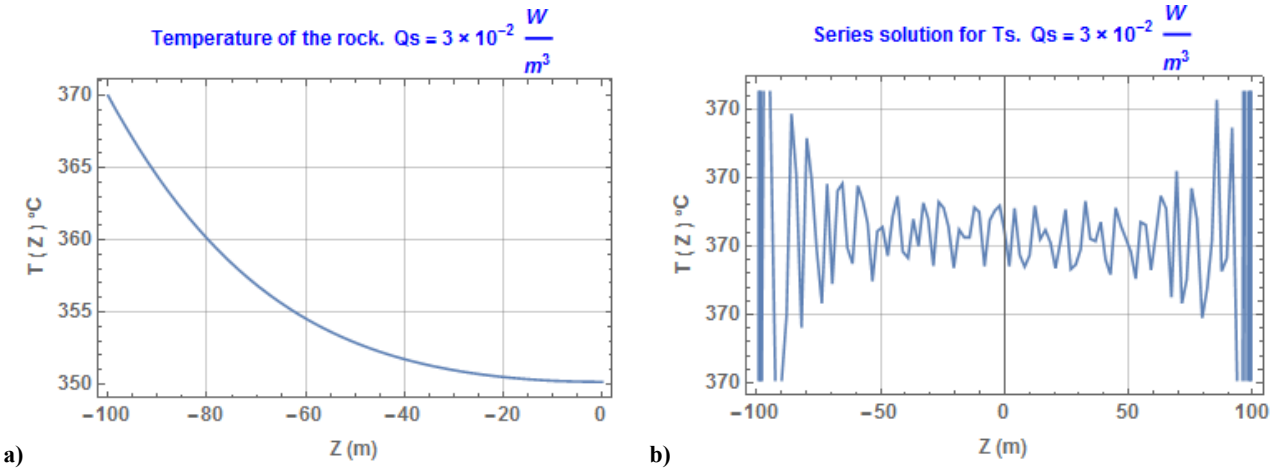

a) b)

Figure 5: a) Infinite series solution of the transient heat flow equation for $t = 65$ years (left), and b) for $t \le 11{,}000$ s (right).

The oscillating behavior of solution (8) shown in Figure 5b, introduces the main point of this paper, which concerns the range of validity of the transient heat flow solution. Even an analytic solution can exhibit divergence and oscillations. Equation (8) fails because it does not represent the real physics of the heat flow at very early times.

2.3 A conduction-convection exact model in 1D

Assuming heterogeneous properties in the fluid-rock system, let V_s and V_f be the elementary volumes representing the solid matrix and the fluid respectively; $V_B = V_s + V_f$ is the bulk volume. Thermal energy is transported by conduction and convection through a corridor represented by a one-dimensional domain of porous rock of volume V_B, as illustrated in figure 6. It is assumed that below and above this domain there is a very low porosity impervious rock of volume V_S, which transfers constant volumetric heat to the upper part of the 1D corridor with fluid flowing with constant velocity v_f.

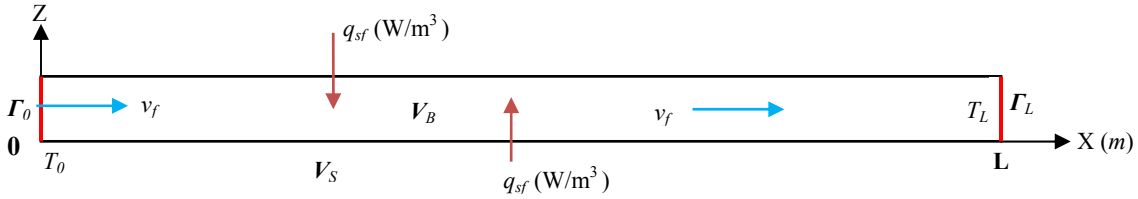

Figure 6: One-dimensional porous rock domain with volumetric heat transfer, Z represents an arbitrary vertical length.

This model idealizes a common situation that occurs when colder water at T_0 °C is injected into a geothermal reservoir at T_L °C, with an important temperature difference ($T_0 << T_L$). The injection well is located at the origin **0** and the fluid migrates to the right a distance **L**. In steady-state the model described by equation (4b) is:

$$\frac{d}{dx}\left(\eta_f \frac{dT_f(x)}{dx}\right) - \frac{v_D}{\varphi}\frac{dT_f(x)}{dx} = -Q_f\,, \quad \left\{ T_f(x=0) = T_0\,,\ T_f(x=L) = T_L \right\},\ \eta_f = \frac{k_f}{c_f \rho_f} \tag{9}$$

where η_f [m^2/s] is the fluid thermal diffusivity. This ordinary linear differential equation for $T_f(x)$ has an exact solution $\tau_f(x)$ in terms of the boundary conditions T_0 and T_L (see Appendix):

$$\tau_f(x) = \frac{\left(\varphi\, Q_f\, L + (T_0 - T_L)\, v_D\right) e^{\frac{v_D\, x}{\varphi\, \eta_f}} - \left(T_0\, v_D + \varphi\, Q_f\, x\right) e^{\frac{v_D\, L}{\varphi\, \eta_f}} + \varphi\, Q_f (x - L) + T_L\, v_D}{\left(1 - e^{v_D L/\varphi\, \eta_f}\right) v_D} \tag{10}$$

Where v_f is the fluid velocity in the pores ($v_f = v_D/\varphi$). Darcy's law is valid for laminar flows where the viscous forces opposing the fluid flow prevail over the inertial forces related to the fluid acceleration. Solution (10) is also valid for non-Darcy fluxes. Some fluid thermal parameters that are needed to make the graphics of this equation are shown in Table 1.

Table 1.- Rock and Fluid Properties for different pressures and temperatures.

Rock Properties	φ (ad) 0.116	$(1-\varphi)$ (ad) 0.884	ρ_s (kg/m^3) 2370	k_s (W/m/°C) 2.14	c_s (J/kg/°C) 1130.4	η_s (m^2/s) 7.99×10^{-7}	d_0 (m) 0.001	
Fluid Properties	**p** (bar)	**T** (°C)	ρ_f (kg/m^3)	k_f (W/m/°C)	c_f (J/kg/°C)	η_f (m^2/s)	μ_f (Pa . s)	***Pr***
1	50	50	990.2	0.6459	4170	15.64×10^{-8}	54.75×10^{-5}	3.54
2	170	350	579.0	0.4498	9683	8.02×10^{-8}	6.64×10^{-5}	1.43
3	220	370	493.0	0.4105	18,190	4.58×10^{-8}	5.67×10^{-5}	2.51

Figures 7 (*a*, *b*, *c*, *d*) show the graphics of the analytic solution (10) for different fluid velocities and heat generations. Figure 8 show the corresponding graphics of $\tau_f(x)$ for different diffusivities. For low fluid velocities (10^{-8} m/s), the fluid in the pores receives enough heat to increase its temperature at a short distance from the injection well. When the fluid velocity increases, the fluid has not enough time to recover heat from the surrounding rock and it arrives to the end of the interval at almost the same injection temperature $T_0 = 50$°C. The fluid temperature behavior is shown in the same figures for increasing heat transfer from 0 up to 0.5 10^{-7} (°C/s).

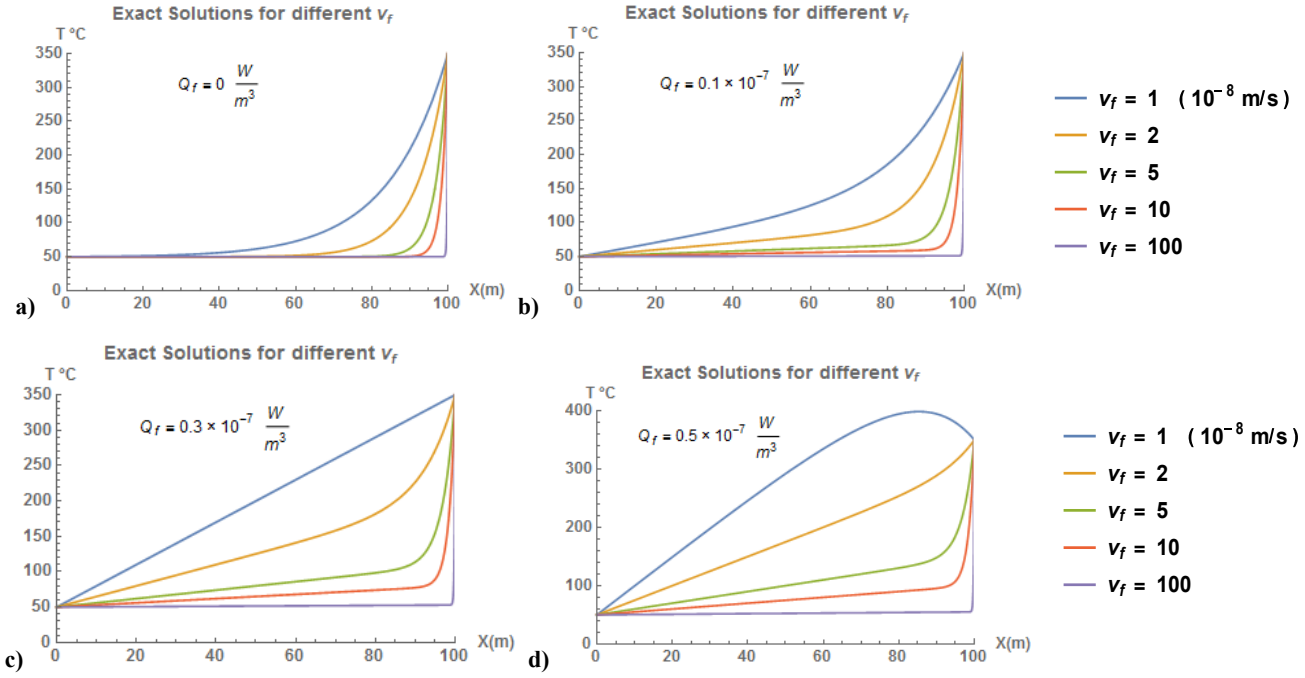

Figure 7: Fluid Temperature distribution for different fluid velocities v_f (10^{-8} m/s), with volumetric heat generation from the solid rock matrix to the fluid Q_f (10^{-7} °C/s), fluid effective diffusivity $\eta = 15.64 \times 10^{-8}$ m^2/s.

The effect of fluid diffusivity on the fluid velocity is noticeable but lower, as can be seen in figures 8a and 8b.

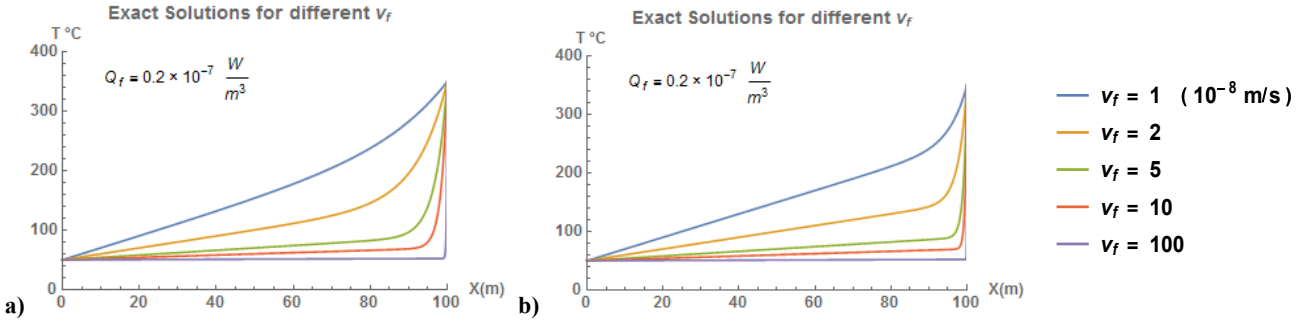

Figure 8: Fluid Temperature distribution for different fluid velocities v_f (10^{-8} m/s), heat generation Q_f = 0.2 × 10^{-7} °C/s , and different fluid diffusivities: a) η_f = 15.64 × 10^{-8} m^2/s, (50 bar, 50 °C); b) η_f = 4.58 × 10^{-8} m^2/s, (220 bar, 370 °C).

It is also interesting to see the fluid temperature profiles for fixed fluid velocity and changing heat flow. This is shown in figures 9 - 10.

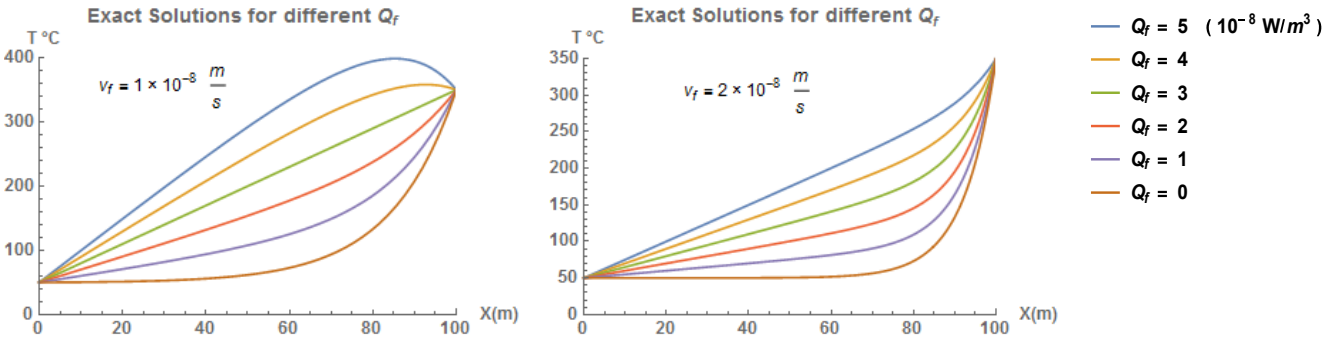

Figure 9: Temperature distribution for different heat transfers at low fluid velocity v_f (10^{-8} m/s), η_f = 15.64 × 10^{-8} m^2/s.

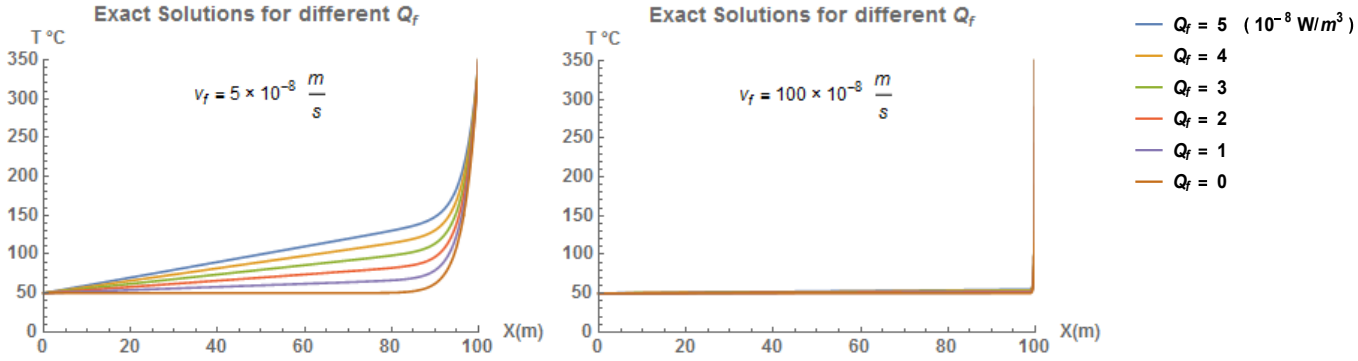

Figure 10: Temperature distribution for increasing heat transfers at high fluid velocity v_f (10^{-8} m/s), η_f = 15.64 × 10^{-8} m^2/s.

From figures 9 and 10, it is clear that the fluid velocity has large effects on the effective volumetric heat transfer from the solid skeleton to the moving fluid for values of Q_f between 3 and 5 × 10^{-8} °C /s. At lower speeds (10^{-8} m/s) the fluid has enough time to recover the thermal energy transferred from the surrounding rock. At this velocity the effective rock-fluid heat transfer is linear or quadratic (Figure 9), inside the interval $0 \leq Z \leq 100$ meters, where the fluid temperature increases smoothly. For larger fluid speeds (10^{-6} m/s), the fluid thermal recovery becomes negligible and the local thermal equilibrium turns from physical reality. The LTE hypothesis appears to be completely wrong for higher fluid velocities in this specific reinjection problem. The only valid thermodynamic state for the approximate correctness of the LTE model is for low fluid velocity or for high v_f combined with a larger rock-fluid energy transfer as is shown in figures 11.

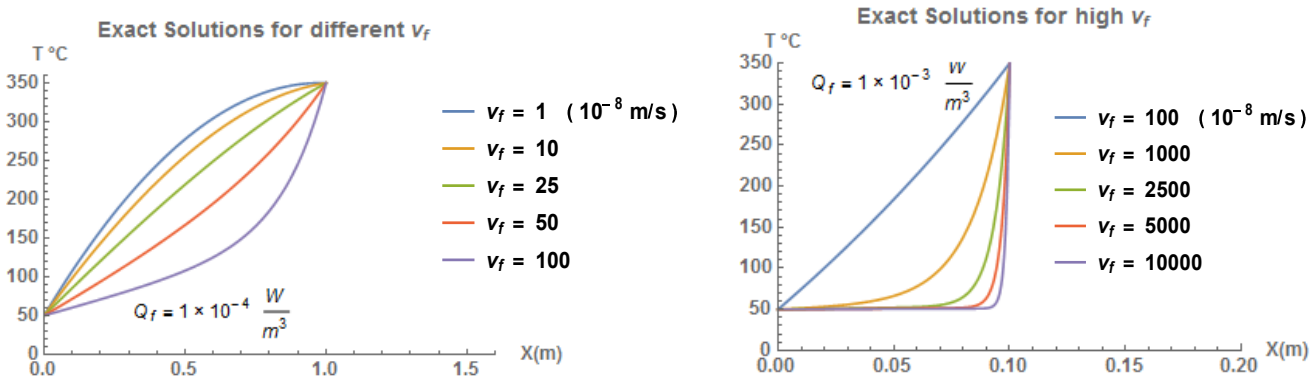

Figure 11: Temperature distributions with large heat transfers at increasing fluid velocity v_f (10^{-8} m/s), $\eta_f = 15.64 \times 10^{-8}$ m²/s.

As can be seen in Figure 11, when the heat transfer increases, the fluid temperature increases within a short distance of 1 meter for different v_f . For a larger heat transfer (10^{-3} °C/s), an approximate local thermal equilibrium is reached within 10 cm.

3. USING THE FINITE VOLUME METHOD TO SOLVE THE CONDUCTION-CONVECTION MODEL

The Method of Integrated Finite Volumes (FVM) is a powerful numerical technique that can be used to solve the partial differential equations of the LTNE model, and is shortly described in the Appendix. The key factor is the approximation of flows at the boundary of each control volume. In the next section the FVM is formulated to solve approximately equations (4a) and (4b) using this technique.

3.1 The Local Thermal Non-Equilibrium Model formulated using Finite Volumes

Assuming homogeneous properties in the fluid-rock system, let V_s and V_f be again the volumes occupied by the solid and the fluid phase respectively in the elementary volume V_n. Integrating the coupled model represented by equation (4) and applying the divergence theorem to the first integral over V_n, two systems of algebraic equations are obtained that approximates the LTNE model:

$$\left(\eta_s \frac{\partial T_s}{\partial \vec{n}} A\right)_{\Gamma_n} = \left(Q_s\, V_n\right),\ \{n=1, N\};\quad \left(\eta_f \frac{\partial T_f}{\partial \vec{n}} A\right)_{\Gamma_n} = \left(\frac{\vec{v}_D \cdot \vec{n}}{\varphi} T_f\, A\right)_{\Gamma_n} - \left(Q_f\, V_n\right),\ \{n=1, N\} \tag{11}$$

where A is the total area of the surface Γ_n overlapping the finite volume V_n of porous rock. The terms inside the parentheses represent average values over the whole surface Γ_n and over each volume $V_n = A\,\delta x_n$ respectively; Q_s, Q_f are the heat exchanged between the solid particles and the fluid in the volume V_n, and N is the total number of finite volumes or nodes composing the computational mesh. A simple one-dimensional mesh is shown in figure 16 (Appendix). Inside the $\{\ V_n\ \}$ domain, local thermal equilibrium is assumed; the temperature of the rock above and below this domain is larger than the fluid temperature in the mesh and there is local thermal non-equilibrium between both zones. The q_{sf} transfer occurs only at this common interface. Computing specific averages for the temperature and fluid properties in equation (11) and assuming equal lateral areas A (right R and left L) for the heat and mass flows between both lateral boundaries $\mathbf{\Gamma}_0$ and $\mathbf{\Gamma}_N$ of the mesh in figure 16:

$$\left(\eta_f \frac{\partial T_f}{\partial n} A\right)_R - \left(\eta_f \frac{\partial T_f}{\partial n} A\right)_L - \left(v_f\, T_f\, A\right)_R + \left(v_f\, T_f\, A\right)_L + Q_f\, A\, \delta x_n = 0$$

$$\Rightarrow\ \eta_{n+1} \frac{T_{n+1} - T_n}{\delta x_{n+1}} - \eta_{n-1} \frac{T_n - T_{n-1}}{\delta x_n} - v_f \left(T_f\right)_R + v_f \left(T_f\right)_L + Q_f\, \delta x_n = 0 \quad ,\ \{n = 2, N-1\} \tag{12}$$

where η_n represent average diffusivity values at the corresponding interface $\{n = 1, N\}$, the boundary conditions at $\mathbf{\Gamma}_0$ and $\mathbf{\Gamma}_N$ are included; $\delta x_n = x_n - x_{n-1}$ is the distance between the center of V_n and the center of V_{n-1}. ($n = 1, N$). The symbols $(T_f)_R$, $(T_f)_L$ represent average values for the changing temperature at each internal boundary Γ_R and Γ_L of each finite volume V_n.

3.1.1 The Weighted Average in the Finite Volume Method

The common weighted general average is:

$$\left(T_f\right)_R = \alpha_R\, T_{n+1} + (1-\alpha_R) T_n\ ,\quad \left(T_f\right)_L = \alpha_L\, T_n + (1-\alpha_L) T_{n-1}\ ;\quad \alpha_L\ ,\ \alpha_R \in [0,1] \tag{13}$$

where $\alpha_L = 1 - \alpha_R$, and $0 \le \alpha_R \le 1$, are weight coefficients representing the influence of the fluid velocity at each boundary. Other type of averages can be used (see Appendix) and the corresponding numerical results are different as is shown in next section.

Using explicitly this average, developing and factorizing the last expression in equation (12), a tridiagonal system of algebraic equations is obtained:

$$\eta_{n+1}\frac{T_{n+1}-T_n}{\delta x_n}-\eta_{n-1}\frac{T_n-T_{n-1}}{\delta x_n}-v_f\left(\alpha_R\,T_{n+1}+(1-\alpha_R)T_n\right)+v_f\left(\alpha_L\,T_n+(1-\alpha_L)T_{n-1}\right)+Q_n\,\delta x_n=0,\{n=2,N-1\} \tag{14}$$

$$\Leftrightarrow \quad \boxed{-a_{n+1}\,T_{n+1}+b_n\,T_n-c_{n-1}\,T_{n-1}=Q_n\,\delta x_n}\ ,\quad \{n=2,N-1\}$$

The boundary conditions for $n = 1$ (T_0) and for $n = N$ (T_L) are computed separately as is shown in the Appendix. Figure 12 shows the non-convergence behavior of this FVM solution for different fluid velocities, using the weighted average formula with two different coefficients $\{\alpha_L, \alpha_R\}$ and the same solid-fluid heat transfer. It is evident that in higher flow dimensions 2D or 3D, this divergence becomes even worst because the directions of the heat flow are more complex and the fluid paths can be more intricate because of tortuosity and other heterogeneities in a real reservoir.

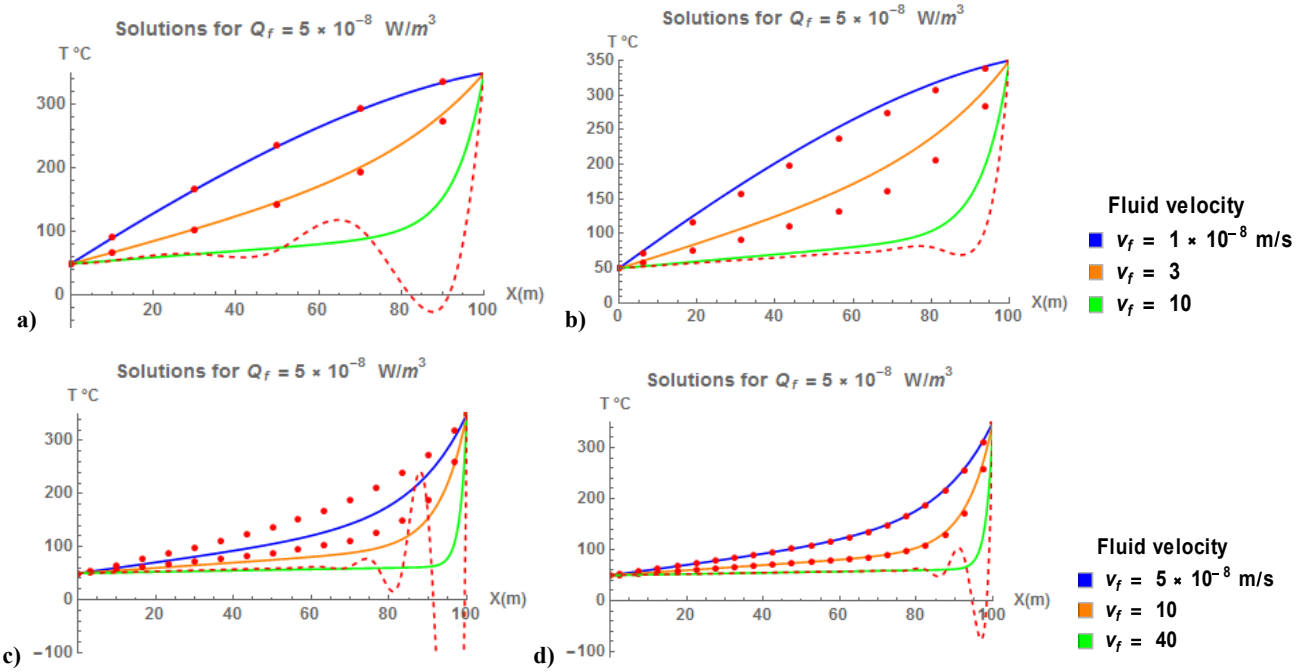

Figure 12: Analytical (continuous line) and Numerical (red dashed line-points) solutions of model (4b) for the fluid temperature profile: a) and d) Arithmetic average ($\alpha_L = \alpha_R = 0.5$); b) and c) are weighted average ($\alpha_L = 1/3$, $\alpha_R = 2/3$) of $T_f(x)$ at the internal boundaries. Both averages produce inaccuracies and/or oscillations about the exact solution when fluid velocity increases.

Using weighted averages, the approximate FVM solution exhibits oscillations without providing accurate approximations specifically at the end of the 1D domain. When the fluid velocity increases from 5 to 50 × 10^{-8} m/s, the oscillations increase in number and the situation becomes worst for larger velocities. The failure of the weighted average in the FVM to simulate combined convection and diffusion flows comes from the fact that this simple average does not recognize the flow direction ($v_f > 0$) in the OX axis nor the strength of convection relative to diffusion as indicated by the Peclet number P_e (Table 1). The following technique, called QUICK, computes non-linear averages of the fluid velocity that can be used in equation (14) to improve the accuracy reducing or eliminating the oscillations.

3.1.2 The QUICK - Leonard Differencing Algorithm in the Finite Volume Method

This is a powerful and stable average formula based on a quadratic interpolation that uses the information of three points at each V_n :

$$-\left(\frac{8\eta_{n+1}}{\delta x_{n+1}}-3\,v_f\right)T_{n+1}+\left(\frac{8\eta_{n+1}}{\delta x_{n+1}}+\frac{8\eta_n}{\delta x_n}+3\,v_f\right)T_n-\left(\frac{8\eta_n}{\delta x_n}+7\,v_f\right)T_{n-1}+v_f\,T_{n-2}=8\,Q_n\,\delta x_n \tag{15}$$

$$\Leftrightarrow \quad \boxed{-a_{n+1}\,T_{n+1}+b_n\,T_n-c_{n-1}\,T_{n-1}+v_f\,T_{n-2}=q_n}\ \geq 0\ ,\quad \{n=2,N-1\}$$

Equation (15) is a tetradiagonal system of algebraic equations, which needs an extra unknown value T_{-1} for $n = 1$ at the Γ_0 boundary. The full system, including the specific calculation of the boundary conditions, are developed in the Appendix. Figure 13 shows the convergence of the corresponding FVM solution for different fluid velocities, using this average formula with different solid-fluid heat transfers. The numerical scheme converges at all tested fluid speeds in every volume V_n. The total number N of nodes and finite volumes can be increased to improve the accuracy of this algorithm for very high fluid speeds (Figures 13c and 13d).

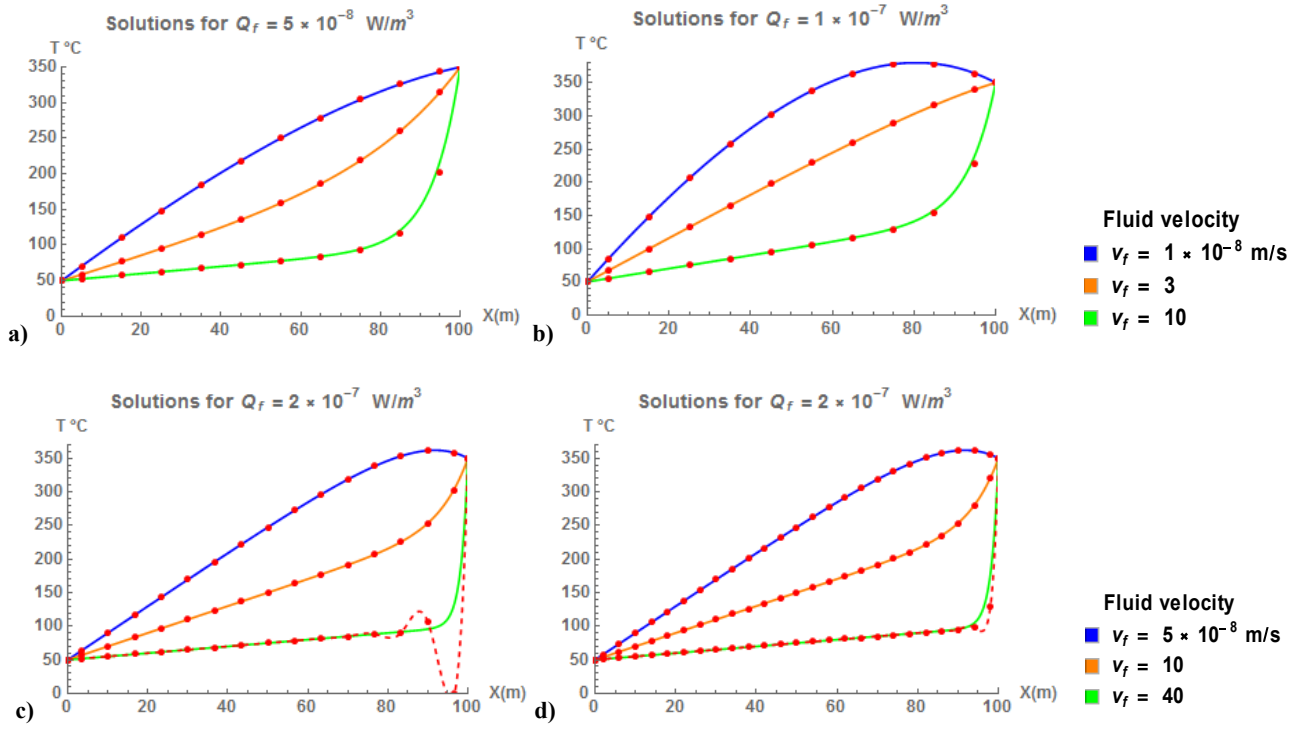

Figure 13: Analytical (continuous line) and Numerical (red points) solutions for the fluid temperature profile using the QUICK-Leonard algorithm and different Q_f (5×10^{-8} and 2×10^{-7} °C /s): a, b) $N = 12$; c) $N = 15$; d) $N = 25$ internal nodes.

It is clear that the QUICK-Leonard algorithm does ***not*** produce oscillations nor inaccuracies at moderate fluid velocities, even in coarse meshes of only 10 nodes; it reproduces the exact solution when fluid velocity increases. For higher fluid velocities ($v_f \geq 4 \times 10^{-7}$ m/s) it exhibits some oscillations at the end of the 1D domain because of the abrupt temperature jump, but the scheme can be corrected easily by increasing moderately the number of finite volumes, as is shown in figure 14. This numerical scheme always works correctly, as is illustrated in the next two figures for the LTNE model at very high fluid velocities.

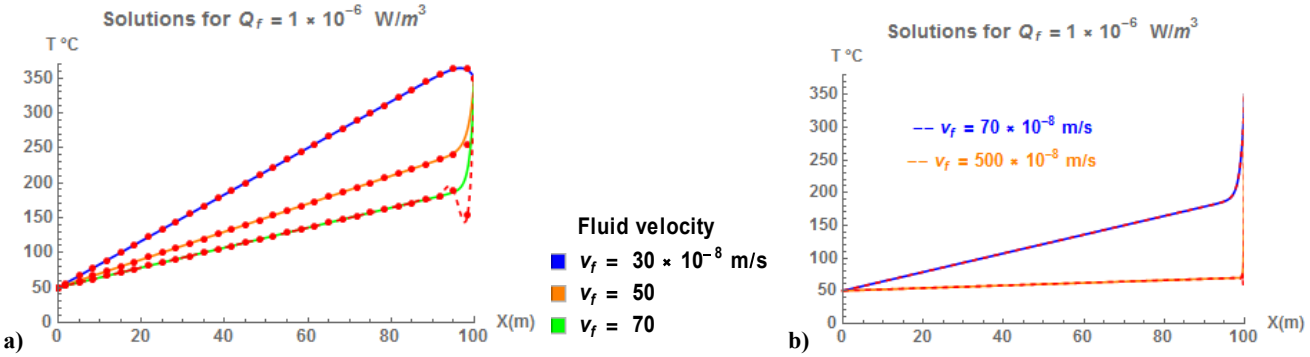

Figure 14: Temperature profiles for high fluid velocities and heat transfers, a) $N = 30$ nodes, b) $N = 200$ nodes .

The non-isothermal groundwater fluid flow illustrated in figure 14b is particularly difficult to simulate for any numerical scheme. The temperature jumps abruptly at the end of the interval for any fluid velocity larger than 10^{-6} m/s, which is a common velocity in porous rocks. The numerical problem occurs because this jump represents an almost mathematical singularity with discontinuous derivatives at the point $Z = 100$ m. The QUICK-Leonard algorithm in the Finite Volume method, reproduces exactly the analytic solution of the conduction-convection model in equation (10) without production of oscillations at the discontinuity point. The numerical scheme

converges in this critical situation using an appropriate *number of nodes*. It provides an efficient differentiation scheme that is physically realistic and numerically stable, which is very appropriate to simulate heat and mass flows in any type of geothermal reservoirs.

4. CONCLUSIONS

The main objective of this work was to provide an explanation and a physical reason for the divergence of a numerical model using the finite volume method. A second objective was to explore the range of validity of the local thermal equilibrium hypothesis during the injection of cold water into a hot reservoir. Using a one-dimensional diffusion-convection model, both objectives were achieved. A numerical model based on the FVM can diverge because of the inappropriate average formula used to compute the fluid velocity at the internal interfaces of the computational mesh. Any discretisation or numerical scheme must satisfy some fundamental properties to simulate the physics of heat and mass flow in a geothermal reservoir. These properties are synthesized in three parts: conservativeness of the physical laws, transportiveness of the fluid flow, and boundedness of the system of algebraic equations. The QUICK-Leonard algorithm posses these three properties, it is very accurate and does ***not*** produce oscillations at normal Darcy velocities. For very high fluid speeds this scheme continues to be convergent by increasing moderately the number of finite volumes. It also works correctly even in the case of an abrupt temperature jump or mathematical singularity with discontinuous derivatives; this scheme converges in this critical situation using an appropriate larger number of nodes. For any other conditions, the FVM can be used to solve general geothermal reservoir engineering problems.

Concerning the validity of the local thermal equilibrium hypothesis, it was shown that the fluid velocity has large effects on the effective volumetric heat transfer from the skeleton to the moving fluid. At lower Darcy speeds (10^{-8} m/s) the fluid has enough time to recover thermal energy from the rock. The LTE hypothesis appears to be completely wrong for higher fluid velocities in the reinjection problem. The only thermodynamic state for the approximate validity of the LTE model is for low fluid velocity with high rock heat transfer. For high fluid velocities the LTE model is appropriate when the solid-fluid energy transfer is large enough.

Porous rocks are coexistent in multiple length scales. Experimental data reveals that there is no unique characteristic length for scaling the relevant dimensionless parameters; more fundamental and experimental research is needed to establish interfacial heat transfer coefficient correlations. The key point in LTNE models is the correct calculation of q_{sf}, h_{sf} and Γ_{sf}. The physical theory and laws that are the basis of the flows in geothermal reservoirs, are supported by both, experiments and equations. The numerical model representing these equations should be coherent with the same physical laws that is supposed to represent in terms of numbers. Therefore, it must be possible to deduce unknown values of a physical property from a pure numerical outcome, based on this coherence.

5. APPENDIX

5.1 Brief Description of the Integrated Finite Volume Method

The Method of Integrated Finite Volumes (FVM) is a powerful technique to solve partial differential equations (PDE) and ordinary differential equations, with numerical approximations using systems of algebraic equations. The FVM is a very versatile technique used in computational fluid dynamics that approaches the solution respecting locally and globally the laws of conservation of mass, momentum, energy and transport of solutes. This property of the FVM is satisfied exactly in every finite volume as well as in the entire computational domain containing any finite number of volumes. In its simplest version, the FVM is similar to the method of finite differences; in its most advanced version it is similar to the finite element method, with a unitary weighting function. The physical domain where the PDE is going to be solved, is represented approximately by a computational mesh formed by simple geometric objects called finite volumes, such as triangles, rectangles, polygons or curved elements (Figure 15). The original PDE is integrated over each volume, but the surface integrals are evaluated as flows through all the boundaries of each element. This numerical method solves the PDE by calculating the average value of the unknown function in each finite volume and averaging the flows at each boundary. This technique applied through the interfaces between adjacent volumes supports the implementation of any formula to compute different averages. This method it is easy to formulate in structured meshes as well as in heterogeneous, unstructured meshes (Figure 15). In the next section the FVM is formulated to solve approximately equations (1) and (2) using this technique.

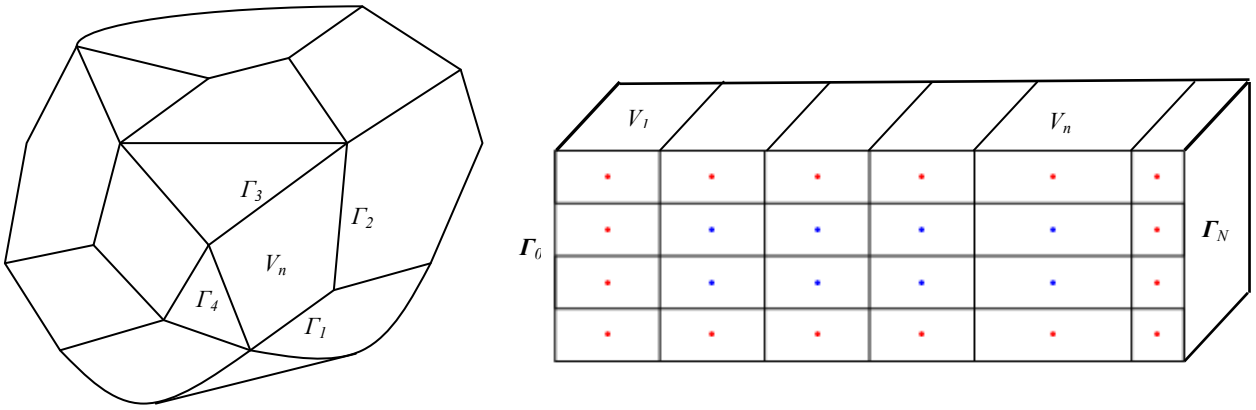

Figure 15: Examples illustrating an unstructured mesh (left) and a structured mesh (right), with boundaries.

5.2 The Local Thermal Non-Equilibrium Model (LTNE) Using the Finite Volume Method in 1D

Assuming homogeneous properties in the fluid-rock system, let V_s and V_f be the volumes occupied by the solid and the fluid phase respectively in the elementary volume V_n. Integrating the model represented by equation (4a) and applying the divergence theorem to the first integral over V_n:

$$\int_{V_n} \vec{\nabla} \cdot \left(\frac{k_s}{c_s \rho_s} \cdot \vec{\nabla} T_s \right) dV_n = \int_{\Gamma_n} \eta_s \vec{\nabla} T_s \cdot \vec{n} \; d\Gamma_n = \int_{V_n} Q_s \; dV_n \;\Rightarrow \left(\eta_s \frac{\partial T_s}{\partial \vec{n}} A \right)_{\Gamma_n} = \left(Q_s \; V_n \right), \;\; n = 1, N \tag{16}$$

Integrating in a similar way the model represented by equation (4b):

$$\begin{aligned} &\int_{V_n} \vec{\nabla} \cdot \left(\frac{k_f}{c_f \rho_f} \cdot \vec{\nabla} T_f \right) dV_n = \int_{\Gamma_n} \eta_f \vec{\nabla} T_f \cdot \vec{n} \; d\Gamma_n = \int_{V_n} \vec{\nabla} \cdot \left(\frac{\vec{v}_D}{\varphi} T_f \right) dV_n - \int_{V_n} Q_f \; dV_n \\ &\Rightarrow \int_{\Gamma_n} \eta_f \frac{\partial T_f}{\partial n} d\Gamma_n = \left(\eta_f \frac{\partial T_f}{\partial \vec{n}} A \right)_{\Gamma_n} = \left(\frac{\vec{v}_D \cdot \vec{n}}{\varphi} T_f \; A \right)_{\Gamma_n} - \left(Q_f \; V_n \right); \;\; n = 1, N \end{aligned} \tag{17}$$

where A is the total lateral area of the surface Γ_n overlapping the finite volume V_n of porous rock. The terms inside the parentheses represent average values over the whole surface Γ_n and over each volume V_n; Q_s and Q_f are the heat exchanged between the solid particles and the fluid in the volume V_n, and N is the total number of finite volumes composing the computational mesh. A simple one-dimensional mesh is shown in figure 16. Inside the 1D domain local thermal equilibrium is assumed; the temperature of the rock above and below this domain is larger than the fluid temperature in the mesh and there is no local thermal equilibrium between both zones (Figure 16).

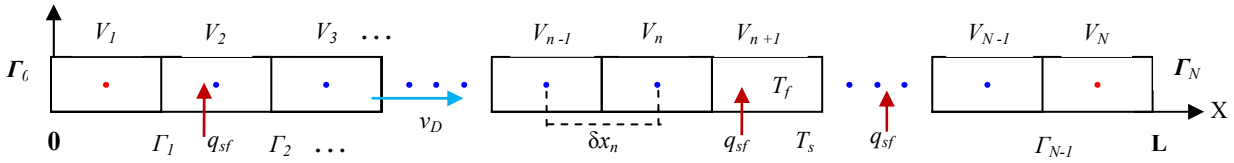

Figure 16: A uniform one-dimensional mesh showing the main elements of the Finite Volume Method: Volumes V_n, internal boundaries Γ_n, internodal distances $\delta x_n = x_n - x_{n-1}$, solid and fluid temperatures ($T_f \neq T_s$) in the LTNE model, the heat transferred from the solid matrix to the fluid q_{sf} and the Darcy velocity v_D in the positive direction OX.

Computing averages for the temperature and fluid diffusivity in equation (17) and assuming equal lateral areas A of each boundary Γ_n (right R and left L) at each finite volume, the heat and mass flows between both boundaries $\mathbf{\Gamma}_0$ and $\mathbf{\Gamma}_N$ in figure 16, the conduction-convection model in terms of the Finite Volume method is as follows:

$$\begin{aligned} &\left(\eta_f \frac{\partial T_f}{\partial x} A \right)_R - \left(\eta_f \frac{\partial T_f}{\partial x} A \right)_L - \left(v_f \, T_f \, A \right)_R + \left(v_f \, T_f \, A \right)_L + Q_f \, A \, \delta x_n = 0 \\ &\eta_{n+1} \frac{T_{n+1} - T_n}{\delta x_{n+1}} - \eta_{n-1} \frac{T_n - T_{n-1}}{\delta x_n} - v_f \left(T_f \right)_R + v_f \left(T_f \right)_L + Q_f \; \delta x_n = 0 \end{aligned} \quad , \quad \left\{ \begin{aligned} \left(T_f \right)_R &= \alpha_R \, T_{n+1} + \left(1 - \alpha_R \right) T_n \\ \left(T_f \right)_L &= \alpha_L \, T_n + \left(1 - \alpha_L \right) T_{n-1} \end{aligned} \right\} \tag{18}$$

where $\delta x_n = x_n - x_{n-1}$ is the distance between the center of volume V_n and the center of volume V_{n-1}, (n = 1, N); δx_n also represents the length of each V_n; the mesh is uniform and the volumes have the same size. The symbols $(T_f)_{R,L}$ represent general weighted averages for the changing temperature at each internal boundary Γ_R (Right) and Γ_L (Left) of each finite volume V_n; η_n represents average diffusivity values at the corresponding interface $\{n = 2, N\text{-}1\}$, the boundary conditions at $\mathbf{\Gamma}_0$ and $\mathbf{\Gamma}_N$ are included below. The pressure gradient in the 1D corridor is assumed linear and therefore the Darcy velocity v_D is constant, and the same for the fluid velocity $v_f = v_D / \varphi$. The computation of the gradient $\partial T_f / \partial x$ at Γ_n uses a central differencing formula because each Γ_n is at the midpoint between x_n and x_{n-1}; therefore the algebraic expression for the normal derivative in equation (18) is second order accurate.

In the next section complete algorithms are shown for different averages. The pure diffusion model for the solid matrix temperature can be obtained in the same way, just by exchanging the subindex f by s and setting $v_f = 0$.

5.3 Some Useful Averages for the Finite Volume Method with Central Differencing Schemes

5.3.1 The General Weighted Average

The weighted average formula is equivalent to a linear interpolation with coefficients (α_L, α_R); the corresponding parallel model is:

$$\eta_{n+1}\frac{T_{n+1}-T_n}{\delta x_n}-\eta_{n-1}\frac{T_n-T_{n-1}}{\delta x_n}-v_f\left(\alpha_R\,T_{n+1}+(1-\alpha_R)T_n\right)+v_f\left(\alpha_L\,T_n+(1-\alpha_L)T_{n-1}\right)+\;Q_n\;\delta x_n=0 \tag{19}$$

where $0 \le \alpha_L \le 1$, $0 \le \alpha_R \le 1$ and $\alpha_L + \alpha_R = 1$. Factorizing the corresponding terms in expression (19), a tridiagonal system of algebraic equations is obtained:

$$\left(\frac{\eta_{n+1}}{\delta x_{n+1}}+\frac{\eta_{n-1}}{\delta x_n}+(1-\alpha_R-\alpha_L)v_f\right)T_n\;=\left(\frac{\eta_{n+1}}{\delta x_{n+1}}-\alpha_R\;v_f\right)T_{n+1}+\left(\frac{\eta_{n-1}}{\delta x_n}+(1-\alpha_L)v_f\right)T_{n-1}+\;Q_n\;\delta x_n$$

$$\Leftrightarrow\qquad \boxed{-a_{n+1}\,T_{n+1}+b_n\,T_n-c_{n-1}\,T_{n-1}\;=\;Q_n\,\delta x_n}\;,\quad \{n\;=\;2\,,N-1\} \tag{20}$$

The corresponding boundary conditions are given by:

$$\left(\frac{\eta_2}{\delta x_2}+\frac{\eta_1}{\delta x_1/2}+\;(1-\alpha_R)\,v_f\right)T_1\;=\left(\frac{\eta_2}{\delta x_2}-\;\alpha_R\;v_f\right)T_2+\left(\frac{\eta_1}{\delta x_1/2}+\;v_f\right)T_0+\;Q_1\;\delta x_1\qquad\rightarrow\;\;\Gamma_0\;\;\{n=1\}$$

$$\left(\frac{\eta_N}{\delta x_N/2}+\frac{\eta_{N-1}}{\delta x_N}-\;\alpha_L\;v_f\right)T_N=\left(\frac{\eta_N}{\delta x_N/2}-\;v_f\right)T_N+\left(\frac{\eta_{N-1}}{\delta x_N}+(1-\alpha_L)\,v_f\right)T_{N-1}+\;Q_N\,\delta x_N\;\rightarrow\;\Gamma_N\;\;\{n=N\} \tag{21}$$

5.3.2 The Arithmetic and Upwind averages:

Many type of averages can be used and the resulting numerical results will be different as is shown in section Y. Using arithmetic averages explicitly by setting $\alpha_L = \alpha_R = 0.5$ in a uniform grid ($\Delta x_{n+1} = \Delta x_n$), factorizing the last expression in equation (14):

$$\left(\frac{\eta_{n+1}+\eta_{n-1}}{\delta x_n}\right)T_n\;=\left(\frac{\eta_{n+1}}{\delta x_n}-\frac{v_f}{2}\right)T_{n+1}+\left(\frac{\eta_{n-1}}{\delta x_n}+\frac{v_f}{2}\right)T_{n-1}+\;Q_n\;\delta x_n\;,\qquad\{n=2\,,N-1\} \tag{22}$$

The Upwind scheme, which identifies directly the flow direction, is defined by setting $\alpha_L = 0$, and $\alpha_R = 1$. The appropriate boundary conditions are easily obtained setting the corresponding values for α_L and α_R in both equations (20, 21). In both cases a tridiagonal system of algebraic equations is obtained:

$$\left(\frac{\eta_{n+1}}{\delta x_{n+1}}+\frac{\eta_{n-1}}{\delta x_n}\right)T_n\;=\left(\frac{\eta_{n+1}}{\delta x_{n+1}}-v_f\right)T_{n+1}+\left(\frac{\eta_{n-1}}{\delta x_n}+v_f\right)T_{n-1}+\;Q_n\;\delta x_n\;,\quad\{n\;=\;2\,,N-1\} \tag{23}$$

Arithmetic, upwind and general weighted averages are only first-order accurate in terms of the truncation error of their corresponding Taylor series. The Upwind scheme is stable but his first-order accuracy makes it inclined to numerical diffusion errors and to need a larger number of volumes in difficult flow problems, as is shown in section 3 of this paper.

5.3.3 The QUICK - Leonard Differencing Scheme

The name QUICK means Quadratic Upstream Interpolation for Convective Kinetics. This scheme was developed by Leonard B. in 1979 using a three point upstream-weighted quadratic interpolation to approximate the values at each finite volume interface. It was reformulated and improved later by Hayase *et al.* (1992), to alleviate some stability problems. It is known as the QUICK-Leonard scheme. The corresponding algorithm, for flow in the positive OX direction ($v_f > 0$), is as follows:

$$\left(T_f\right)_R=\;\frac{3}{8}\,T_{n+1}+\;\frac{6}{8}\,T_n-\;\frac{1}{8}\,T_{n-1}\;,\quad\left(T_f\right)_L=\;\frac{3}{8}\,T_n+\;\frac{6}{8}\,T_{n-1}-\frac{1}{8}\,T_{n-2} \tag{24}$$

where the terms in parentheses are the average values of the temperature at each internal boundary Γ_n. Replacing these values in equation (18) and factorizing, a tetra-diagonal system of algebraic equations is obtained:

$$-\left(\frac{8\eta_{n+1}}{\delta x_{n+1}}-3\,v_f\right)T_{n+1}+\left(\frac{8\eta_{n+1}}{\delta x_{n+1}}+\frac{8\eta_n}{\delta x_n}+3\,v_f\right)T_n-\left(\frac{8\eta_n}{\delta x_n}+7\,v_f\right)T_{n-1}+v_f\,T_{n-2}=\,8\,Q_n\,\delta x_n$$

$$\Leftrightarrow\qquad \boxed{-a_{n+1}\,T_{n+1}+b_n\,T_n-c_{n-1}\,T_{n-1}+v_f\,T_{n-2}=\,8\,Q_n\,\delta x_n=q_n}\;\geq\;0\,,\quad \{n\;=\;2\,,N-1\} \tag{25}$$

For $n = 1$, a T_{-1} unknown value at boundary $\boldsymbol{\Gamma}_0$ is needed at the left side (x_{-1}) of the first node corresponding to $(T_f)_L$ in equation (25). This value is calculated by linear extrapolation between nodes (x_1) and (x_0) separated by a distance $\delta x_n/2$, which gives $T_{-1} = 2\,T_0 - T_1$. To obtain consistency with this formula, the normal derivatives of T_f at both boundaries $\boldsymbol{\Gamma}_0$ and $\boldsymbol{\Gamma}_N$, are calculated differently:

$$\left(T_f\right)_{\Gamma_0}=\frac{7}{8}\,T_1+\frac{3}{8}\,T_2-\frac{2}{8}\,T_0\,,\;\left(\eta_f\,\frac{dT_f}{dx}\right)_{\Gamma_0}=\frac{\eta_0}{3\,\delta x}\left(9\,T_1-T_2-8\,T_0\right),\;\left(\eta_f\,\frac{dT_f}{dx}\right)_{\Gamma_N}=\frac{\eta_N}{3\,\delta x_N}\left(8\,T_{\rm N}-9\,T_{\rm n}+T_{n-1}\right) \tag{26}$$

Thus, the corresponding boundary conditions at $\boldsymbol{\Gamma}_0$ ($n = 1$) and $\boldsymbol{\Gamma}_N$ ($n = N$) are given by the following equations:

$$\begin{aligned}
&-\left(\frac{8\eta_2}{\delta x_2}+\frac{8\eta_0}{3\,\delta x_1}-3\,v_f\right)T_2+\left(\frac{8\eta_2}{\delta x_2}+\frac{24\eta_0}{\delta x_1}+7\,v_f\right)T_1\;=\left(\frac{64\eta_0}{3\,\delta x_1}+10\,v_f\right)T_0+8\,Q_1\,\delta x_1 &&\rightarrow\;\boldsymbol{\Gamma}_0\\
&-\left(\frac{8\eta_N}{\delta x_n}+\frac{8\eta_{n-1}}{\delta x_{n-1}}+6\,v_f\right)T_{n-1}+\left(\frac{24\eta_N}{\delta x_n}+\frac{8\eta_{n-1}}{\delta x_{n-1}}-3\,v_f\right)T_n+v_f\,T_{n-2}=\left(\frac{64\eta_N}{3\,\delta x_n}-8\,v_f\right)T_N+8\,Q_n\,\delta x_n &&\rightarrow\;\boldsymbol{\Gamma}_N
\end{aligned} \tag{27}$$

The left interface of volume V_2 is the right boundary of volume V_1, and is also affected by the extrapolation in equation (26); to assure consistency with this approximation, a similar average is done for $n = 2$:

$$-\left(\frac{8\eta_3}{\delta x_3}-3\,v_f\right)T_3+\left(\frac{8\eta_2}{\delta x_2}+\frac{8\eta_1}{\delta x_1}+3\,v_f\right)T_2-\left(\frac{8\eta_1}{\delta x_1}+8\,v_f\right)T_1=\,-2\,v_f\,T_0+8\,Q_2\,\delta x_2 \tag{28}$$

The QUICK-Leonard algorithm is very stable and minimizes numerical diffusion errors; it uses a higher order interpolation technique with three neighbor points, which bring a wider influence of the data to compute the average values of T_f at each interface. This scheme comes from a quadratic function passing through the central points of three volumes, two on both sides of each boundary and another one on the upstream side. Therefore it takes into account the real flow direction and is completely adequate to model flows in geothermal reservoirs using the finite volume method.

5.4 Exact Solution of the one-dimensional conduction-convection model

In steady-state the model described by equation (4b) is:

$$\frac{d}{dx}\left(\frac{k_f}{c_f\,\rho_f}\,\frac{dT_f(x)}{dx}\right)-\frac{v_D}{\varphi}\,\frac{dT_f(x)}{dx}=-\,Q_f\;,\quad\left\{\,T_f(x=0)=T_0\;,\;T_f(x=L)=T_L\,\right\} \tag{29}$$

Integrating equation (29) once, assuming that porosity, diffusivity and Darcy velocity are constants:

$$\eta_f\,\frac{dT_f(x)}{dx}-\frac{v_D}{\varphi}\,T_f(x)=-\,Q_f\,x+C_0\;\Leftrightarrow\;\frac{dT_f(x)}{dx}-\frac{v_f}{\eta_f}\,T_f(x)=-\frac{Q_f}{\eta_f}\,x+\frac{C_0}{\eta_f},\quad\eta_f=\frac{k_f}{c_f\,\rho_f}\;\left[\frac{m^2}{s}\right] \tag{30}$$

where η_f is the fluid thermal diffusivity and C_0 is an arbitrary integration constant, v_f is the fluid velocity in the pores ($v_f = v_D/\varphi$) and v_D is the macroscopic Darcy velocity. This is an ordinary linear differential equation of the function $T_f(x)$, which has an exact solution $\tau_f(x)$ in terms of the boundary conditions T_0 and T_L. An obvious integrating factor of this linear equation is $\lambda\,(x)$:

$$\begin{aligned}
&\lambda(x)=e^{-\int\frac{v_f}{\eta_f}\,dx}=e^{-\frac{v_f}{\eta_f}x}\;\Rightarrow\;\frac{dT_f(x)}{dx}\lambda(x)-\frac{v_f}{\eta_f}\lambda(x)\;T_f(x)=-\frac{Q_f}{\eta_f}\,x\,\lambda(x)+\frac{C_0}{\eta_f}\lambda(x)\;\Leftrightarrow\\
&d\left(T_f(x)e^{-\frac{v_f}{\eta_f}x}\right)=\left(-\frac{Q_f}{\eta_f}\,x+\frac{C_0}{\eta_f}\right)e^{-\frac{v_f}{\eta_f}x}\;\Rightarrow\;T_f(x)e^{-\frac{v_f}{\eta_f}x}=\int\left(-\frac{Q_f}{\eta_f}\,x+\frac{C_0}{\eta_f}\right)e^{-\frac{v_f}{\eta_f}x}\,dx+C_1
\end{aligned} \tag{31}$$

where C_1 is a second arbitrary integration constant. Replacing the boundary conditions T_0, T_L and factorizing:

$$\tau_f(x) = \frac{\left(e^{v_f x/\eta_f} - 1\right) L\, Q_f + e^{v_f x/\eta_f}\left(T_0 - T_L\right) v_f + T_L\, v_f + Q_f\, x - e^{L v_f/\eta_f}\left(T_0\, v_f + Q_f\, x\right)}{\left(1 - e^{L v_f/\eta_f}\right) v_f} \tag{32}$$

Replacing the fluid velocity by the Darcy velocity ($v_f = v_D/\varphi$) the final expression (10) is obtained.

$$\tau_f(x) = \frac{\left(\varphi\, Q_f\, L + \left(T_0 - T_L\right) v_D\right) e^{\frac{v_D x}{\varphi\,\eta_f}} - \left(T_0\, v_D + \varphi\, Q_f\, x\right) e^{\frac{v_D L}{\varphi\,\eta_f}} + \varphi\, Q_f\left(x - L\right) + T_L\, v_D}{\left(1 - e^{v_D L/\varphi\,\eta_f}\right) v_D} \tag{33}$$

where v_f is the fluid velocity in the pores ($v_f = v_D/\varphi$). If the heat transfer is any function of x, $Q_f(x)$, the procedure described in this section to obtain equation (32) is still valid, the only change is in the last integration of equation (31).

REFERENCES

Bai, M., Elsworth, D. and Roegiers, J.-C.: Multiporosity/multipermeability approach to the simulation of naturally fractured reservoirs. *Water Resour. Res.* 29:6 (1993), pp. 1621–1633.

Bundschuh, J. and Suarez-Arriaga, M.C.: Introduction to the Numerical Modeling of Groundwater and Geothermal Systems – Fundamentals of mass, energy and solute transport in poroelastic rocks. Vol. 2, Multiphysics Modeling Series, CRC Press – Taylor & Francis Group (2010).

Carslaw, H.S. and Jaeger, J.C.: *Conduction of heat in solids*. 2nd ed, Oxford Clarendon Press, Oxford, UK, 1959.

Cinco Ley, H. and Meng, H.Z.: Pressure transient analysis of wells with finite conductivity fractures in double porosity reservoirs. Paper SPE 6019 presented at the SPE Annual technical Conference and Exhibition, New Orleans, Oct. 3–6, 1988.

Hayase, T., Humprey, J.A.C. and Greif, R.: A Consistently Formulated QUICK Scheme for Fast and Stable Convergence Using Finite-Volume Iterative Calculation Procedures, *Journal of Computational Physics*, **98**, (1992), 108-118.

Leonard, B.P.: A Stable and Accurate Convective Modeling Procedure Based on Quadratic Upstream Interpolation, *Computational Methods Appl. Mechanics Engineering,* **19**, (1979), 59-98.

Narasimhan, T. and Witherspoon, P.: An integrated finite difference method for analyzing fluid flow in porous media. Water Resources Res. **12**:1 (1976), 57–64.

Nield, D.A., and Bejan, A.: Convection in Porous Media, Springer Science, New York (2013).

Patankar, S.V.: Numerical Heat Transfer and Fluid Flow, Hemisphere Publishing Corporation, Taylor & Francis Group, New York (1980).

Pruess, K.: SHAFT, MULKOM, TOUGH: A set of numerical simulators for multiphase fluid and heat flow. *Geotermia* **4**:1 (1988), 185–202.

Suárez Arriaga, M.C.: The interfacial interaction problem in complex multiple porosity fractured reservoirs., *Seventh Granada Lectures, AIP Conference Proceedings*, **661 (**2003), American Institute of Physics, New York, NY.

Vafai, K., (editor): Handbook of Porous Media, *CRC Press* – Taylor & Francis Group (2015).